Silicon (2019) 11:1235–1246
https://doi.org/10.1007/s12633-018-9885-1

ORIGINAL PAPER

# Density Functional Theory Study on the Mechanical Properties and Interlayer Interactions of Multi-layer Graphene: Carbonic, Silicon-Carbide and Silicene Graphene-like Structures

**Morteza Ghorbanzadeh Ahangari[1] · Azam Salmankhani[2] · Amir Hossein Imani[1] · Navid Shahab[3] · Amin Hamed Mashhadzadeh[3]**

Received: 25 May 2017 / Accepted: 23 April 2018 / Published online: 22 June 2018


**Abstract**
The main purpose of this study is to calculate the Young's modulus of carbonic (c-graphene), silicon-carbide (SiC) and silicene graphene-like structures using density functional theory (DFT). Our results show that an increase in the number of layers did not noticeably change the Young's modulus of carbonic and silicon-carbide graphene, while the Young's modulus of silicene sheets decreased. Moreover, we found that carbonic graphene had the highest Young's modulus among the above-mentioned graphene sheets due to having the shortest distance between its elements. In contrast, silicene graphenes had the lowest mechanical properties and highest equilibrium Si-Si distance. We also investigated the existing van der Waals interfacial interaction between the layers of the multilayer graphene structure using the Lennard-Jones potential. We used the Lennard-Jones parameters ($\varepsilon$ and $\sigma$) to model the van der Waals interaction as a classical linear spring. Finally, the densities of states (DOS) were calculated to better understand the electronic properties of these systems.

**Keywords** DFT · Graphene · Silicene · Silicon-Carbide · Young's modulus

## 1 Introduction

The amazing properties of nano-based carbon allotropes such as nanotubes [1], graphenes [2, 3] and fullerenes [4] have attracted researchers' attention for their use in different applications. CNTs are known as perhaps the most popular nano-based carbon allotropes, but the high production cost of this material has limited its usage in some applications. Graphene was discovered by a group of researchers from Manchester University in 2004 [2]. They used micro-mechanical cleavage to extract individual layers of carbon atoms (monolayer sheets) from graphite. Graphene is possibly the best alternative to CNTs; Nicholas A. Kotov [5] mentioned in his review that "when carbon fibers just will not do, but nanotubes are too expensive, where can cost-conscious materials scientists go to find a practical conductive composite? The answer could lie with graphene sheets". Graphene, which is defined as a single atomic layer of graphite, has a two-dimensional and crystalline structure [6, 7]. This material has a high potential for use in different applications such as nanocomposite based-polymers [8–15], sensors [16], super-capacitors [17], adsorbents [3] and batteries [18]. For example, the use of graphene as reinforcements in polymers creates covalent and non-covalent interactions in the combination of graphene and polymer [19], which gives rise to an enhancement of the mechanical properties of the polymer matrix [20].

The ideal structure for carbon is a honeycomb lattice because the four valence electrons per carbon atom are exactly enough to fill all of the bonding electronic orbitals but none of the anti-bonding orbitals [21]. Because graphene is constructed from the lightest element of group IV of the periodic table, it is natural to consider the possibility of heavier graphene analogues [22]. These heavier post-carbon group IV elements have great potential for the construction of honeycomb structures [22]. Post-carbon

✉ Amin Hamed Mashhadzadeh
amin.hamed.m@gmail.com;
amin.hamedmashhadzadeh@yahoo.com

[1] Department of Mechanical Engineering, Faculty of Engineering and Technology, University of Mazandaran, Babolsar, Iran

[2] Department of Mechancial Engineering, KN University of Technology, Tehran, Iran

[3] Department of Mechanical Engineering, Sari Branch, Islamic Azad University, Sari, Iran

group IV elements such as silicon, germanium and tin have two-dimensional (2D) stable honeycomb structures known as silicene, germanene and stanene, which show chemical behavior that is similar to that of carbon in various aspects [23] because the electronic configurations of silicon, germanium and tin are similar to carbon [21] In recent decades, many researchers have experimentally and theoretically studied the properties of silicene. Silicene was first predicted by an ab initio method in 1994 and has recently been experimentally synthesized over silver (110) and (111) substrates [24–26]. Silicene has a high ability to react with the surface of materials because, unlike graphene, silicene is not stable as a perfectly planar sheet and has chair-like distortions in the rings [27] $Sp^2$ hybridization is energetically favorable in carbonic graphene, while in silicene, $sp^3$ hybridization is more stable. On the other hand, the electronic properties of silicene are similar to those of carbonic graphene because it is a semi-metallic material. Although Si and C have great potential for mixing with each other and forming a 2D layered or nanotube structure (namely, silicon-carbide), silicon-carbide has unusual properties that are unlike those of carbonic graphene because silicon-carbide is polar. For example, a silicon-carbide monolayer sheet exhibits a semiconductor band structure, while carbonic graphene is known as a zero band gap semimetal [28]. Furthermore, some other typical properties of SiC that are of interest for researchers world-wide include its high thermal conductivity, wide band gap and radiation resistance [29] However, experimental processes for the evaluation of the properties of nanomaterials and especially the mechanical properties are costly, and additionally, it is not possible to synthesize some nano-structures, motivating the use of computational simulation methods for the study of the behavior of these materials.

Various atomistic simulation methods such as classical Monte Carlo, ab initio quantum mechanics, molecular dynamics and semi-empirical methods have been used to investigate the adsorption [30], mechanical [31] and electronic properties [32] of nanomaterials such as CNTs [33], graphenes [34], B-N nanotubes (BNNTs) [35], graphidyne [3] or other existing nanocomposites [27]. Among these methods, the results obtained from ab initio quantum mechanics either based on Hartree-Fock (H-F) or density functional theory (DFT) are in closer agreement with the experimental data [32].

This work aims to compare the Young's modulus of mono-, bi- and trilayer carbonic, silicon-carbide and silicene graphene-like structures using the DFT method. We also investigated the van der Waals interfacial interaction between the layers of the multilayer graphene structure using the Lennard-Jones potential. Then, Lennard-Jones parameters were used to model the interaction by classical linear springs. Finally, we generated the density of state diagrams of desired nano materials to understand their electronic properties.

## 2 Computational Method

The atomic geometry and electronic structure of multilayer carbonic, SiC and silicene graphenes were calculated using an ab initio DFT framework [36, 37] and executed using the Spanish Initiative for Electronic Simulations with Thousands of Atoms (SIESTA) code [38, 39]. We adopted the generalized-gradient approximation (GGA) function with the Perdew-Burke-Ernzerhof (PBE) to treat the effects of correlation and electronic exchange. In all procedures, the selected atomic orbital basis sets were double-$\zeta$ plus polarization orbitals (DZP) with an energy shift of 50 MeV and a split norm of 0.3. A $5 \times 5 \times 1$ Monkhorst- Pack grid was used for the k-point sampling of the Brillouin zone, and the atomic positions were relaxed until the residual forces on each atom were lower than 0.03 $eVÅ^{-1}$ [40, 41]. Periodic boundary conditions were used with the $6 \times 6$ supercells containing 50 atoms in each layer. The vacuum height was set to 20 Å to ensure that the z-axis of the periodic supercell is large enough and to eliminate the spurious interaction between the periodically repeated images of multilayer

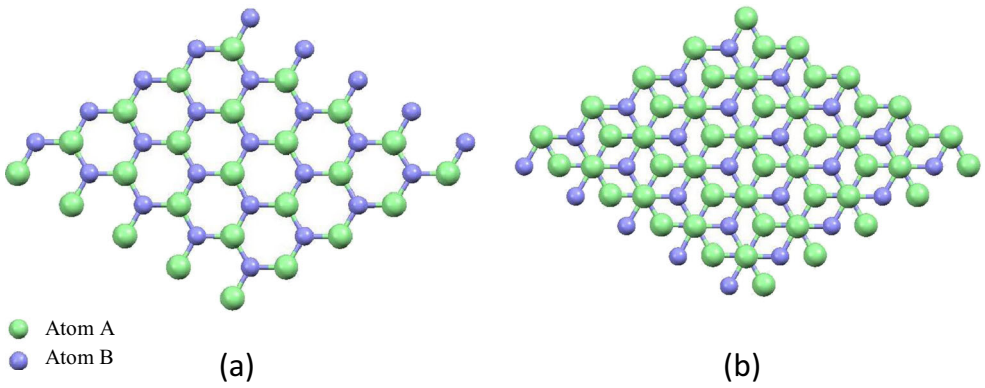


**Fig. 1** Geometric structures of (C-graphene, SiC and Sillicen) bilayers graphene with **a** AA and **b** AB stacking pattern

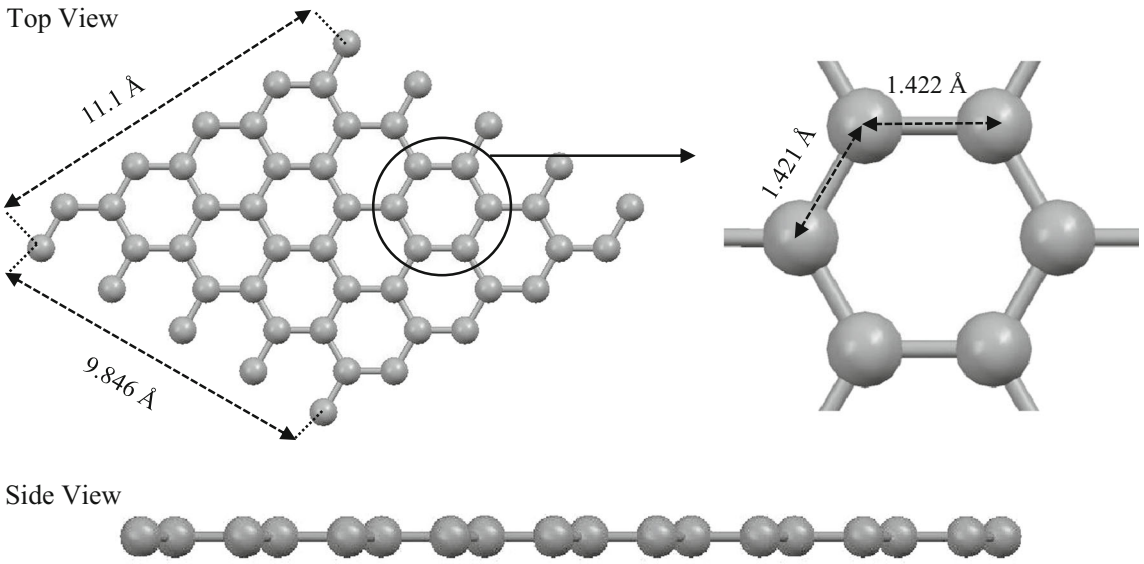


**Fig. 2** Optimized structure and geometrical parameters of bare carbonic graphene sheet

graphene [42]. The mesh cutoff, the energy that corresponds to the grid spacing, was selected as 120 Ry. To determine the stabilities of multilayer graphene, the binding energies ($E_{BG}$) are calculated as:

$$E_{BG} = (E_{MG} - nE_{SG}), \quad (1)$$

where $E_{MG}$ is the total energy of the multilayer graphene, $E_{SG}$ is the energy for the single layer graphene and $n$ is the number of graphene layers [42].

## 3 Results and Discussion

To study the interlayer properties of carbonic, SiC and silicene graphenes, we assumed two arrangements as shown in Fig. 1 [43, 44]. Figure 1a displays the AA stacking pattern for which the A (B) atom of the upper layer is located on the surface of the A (B) atom of the lower graphene layer. In the other arrangement (AB stacking pattern) (Fig. 1b), the A atoms of upper layer are situated on the center of the hexagonal rings of the lower monolayer sheet. In other words, in the AB stacking pattern, the A (B) atoms of the upper layer are located on the B (A) atom of the substrate graphene sheet.

### 3.1 Carbonic Graphene

First, we optimized the geometric parameters of C-graphene as shown in Fig. 2. Examination of this figure shows that the equilibrium length of the C-C bond is approximately 1.42 Å. Examination of the results obtained in previous studies reveals that the calculated bond length between two carbon atoms in the structure of C-graphene is in good agreement with other atomistic simulation methods such as DFT-generalized gradient approximation (1.426 Å), DFT-local density approximation (1.414 Å), the AIREBO potential (1.41 Å), the Tersoff potential (1.464 Å) and the EDIP-Marks potential (1.42 Å) [45]. Furthermore, Novoselov et al. [2] experimentally investigated thin carbon films and reported that the C-C bond length in graphene was approximately 1.42 Å. Hence, our DFT results are also in good agreement with the experimental results.

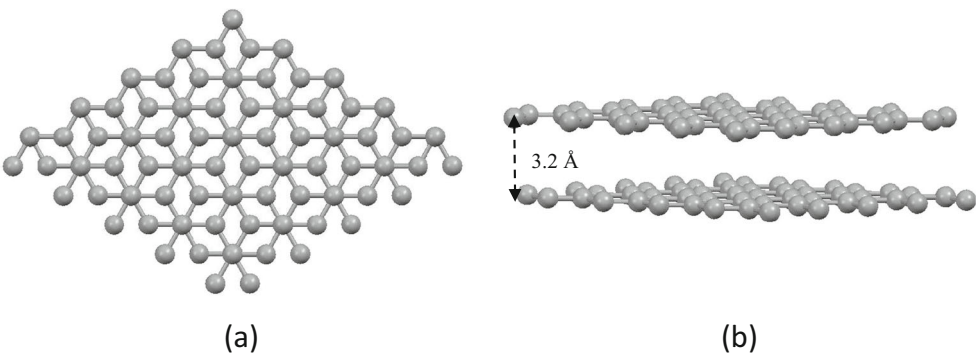


**Fig. 3** Optimized structure and geometrical parameters of C-graphene bilayers **a** top view and **b** side view

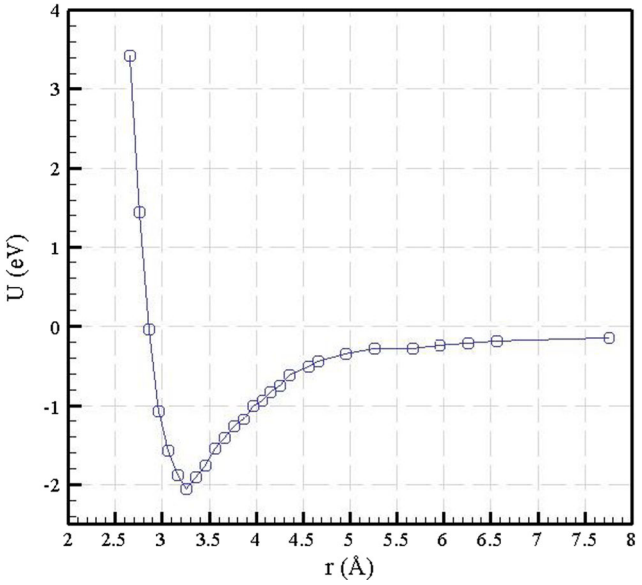


**Fig. 4** Potential energy of two monolayer sheets in structure of C-graphene bilayers as a function of separation distance

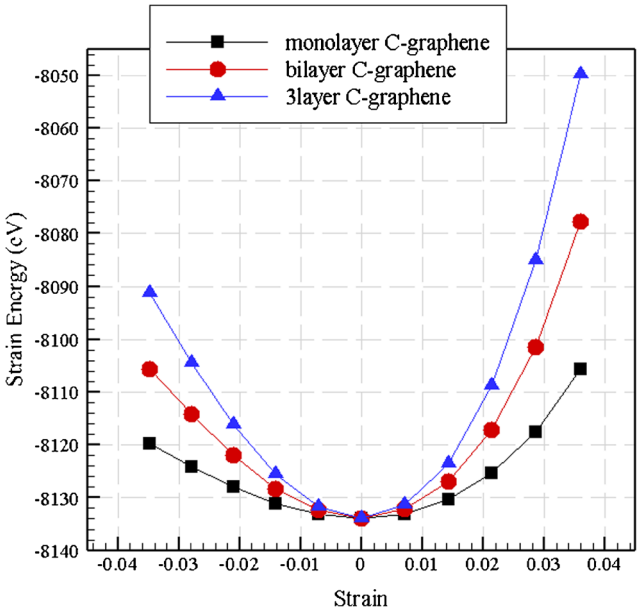


**Fig. 6** Strain energy versus strain for uniaxial strain in monolayer, bilayers and 3layers carbonic graphene sheets

The dimensions of carbonic graphene in this study were considered equal to 11.1 Å × 9.846 Å.

In next section, another C-graphene was located on the surface of the carbonic monolayer sheet in the two arrangements mentioned above. We found that the lowest energy obtained for the two-layer graphite in the AA stacking pattern was approximately -0.012 eV/bond based on DFT calculations, while the greatest exothermic energy in the AB stacking pattern was approximately -0.018 eV/bond. These results clearly show that graphene sheet layers tend to be placed in the AB pattern. Figure 3 displays the most stable orientation on the C-graphene bilayers. It can be seen that the lowest distance between the layers in the C-graphene bilayer structure was approximately 3.2 Å. Jafari et al. [40] investigated the properties of adsorption of platinum by carbonic graphene using DFT calculation. They found that the equilibrium distance between the graphene layers in the graphite structure was approximately 3.351 Å, which is close to our results. In another study, Ghorbanzadeh et al. [46] reported that the distance between the graphene layers in the optimized structure was approximately 3.2 Å.

The above results show that interfacial van der Waals interaction is present between the layers in C-graphene bilayers, which can be modeled using the Lennard-Jones potential form given by:

$$U(r) = 4\varepsilon\left[\left(\frac{\sigma}{r}\right)^{12} - \left(\frac{\sigma}{r}\right)^{6}\right], \tag{2}$$

where $U(r)$ is the potential energy between the single layer C-graphene sheets, $r$ and $\varepsilon$ are the distance and strength, respectively, of the interaction between the monolayer sheets and $\sigma$ is the van der Waals separation distance. For this potential, the minimum potential energy between the two layers of bilayer graphene is found for the smallest distance between them (equilibrium distance). Therefore, the first derivative of this equation, which gives the van der Waals force $(F(r))$, is equal to zero. The expression for $F(r) = dU(r)/dr$ is obtained by differentiating the

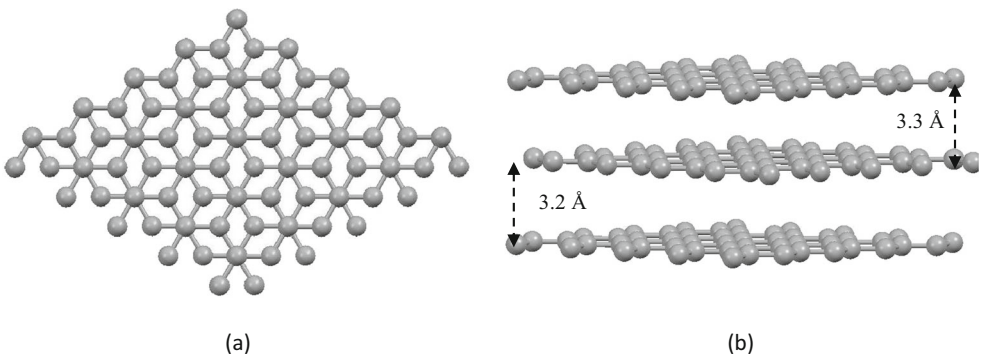


**Fig. 5** Optimized structure and geometrical parameters of C-graphene 3layers **a** top view and **b** side view

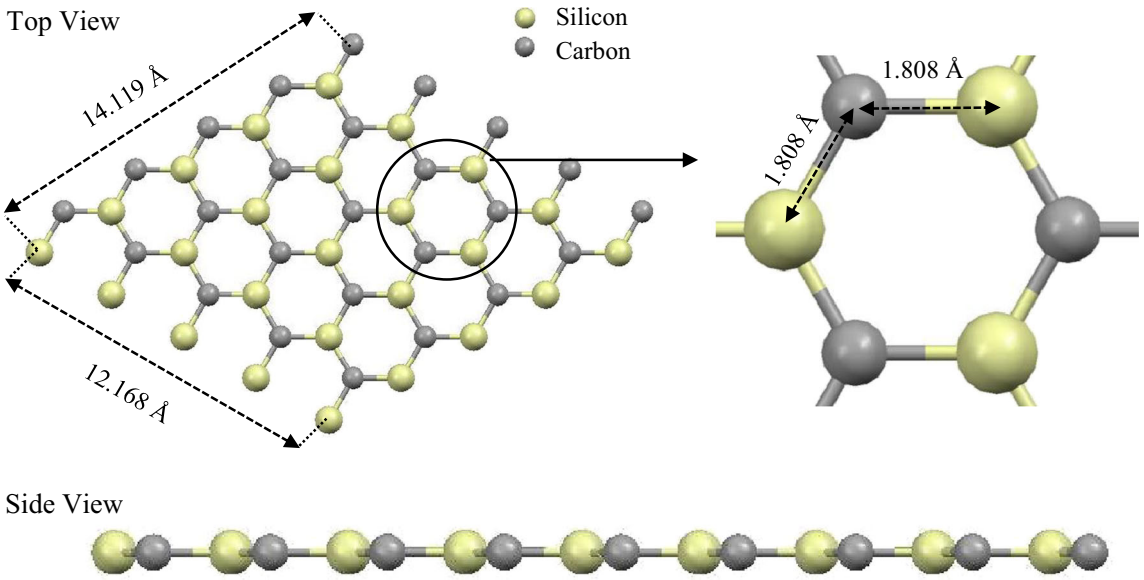


**Fig. 7** Optimized structure and geometrical parameters of SiC-graphene monolayer sheets **a** top view and **b** side view

expression for the Lennard-Jones potential, and then, $r_{eq}$ is determined by setting this expression to zero.

$$F(r) = \frac{dU(r)}{dr} = \frac{24\varepsilon}{r}\left[-2\left(\frac{\sigma}{r}\right)^{12} + \left(\frac{\sigma}{r}\right)^{6}\right] \tag{3}$$

$$F(r) = 0 \qquad r_{eq} = 2^{1/6}\sigma \tag{4}$$

Thus, the Lennard-Jones parameter $\sigma$ can be calculated as:

$$\sigma = 2^{-1/6} r_{eq} \tag{5}$$

Furthermore, we can calculate the value of the Lennard-Jones parameter $\varepsilon$ by obtaining the potential energy at the minimum, according to:

$$U(r_{eq} = -\varepsilon) \tag{6}$$

We determined the Lennard-Jones parameter by changing the distance between the layers of the C-graphene bilayer and fitting the curve of the potential energy between these monolayers of C-graphene as a function of the separation distance as shown in Fig. 4. The Lennard-Jones parameter $\varepsilon$ and $\sigma$ values for mentioned graphene were approximately -2.05 eV and 2.86 Å, respectively.

Next, a monolayer carbonic graphene was placed on the surface of the C-graphene bilayers to study the mechanical and electronic properties of the C-graphene trilayers. Figure 5 shows the optimized structure of trilayer C-graphene. It can be seen from the figure that the third layer was located at a distance of 3.3 Å for trilayer C-graphene. Furthermore, the adsorbed energy of the third layer was calculated and was found to be equal to −0.023 eV/bond according to Eq. 1.

We also calculated the Young's modulus of the monolayer, bilayers and trilayers of carbonic graphene. For this purpose, all of these graphenes were compressed and then elongated along the $x$ direction with a small increment (1.00709 Å), and the strain energy for each strain value was plotted as shown in Fig. 6. The Young's modulus can be calculated as the second derivative of the total energy of the

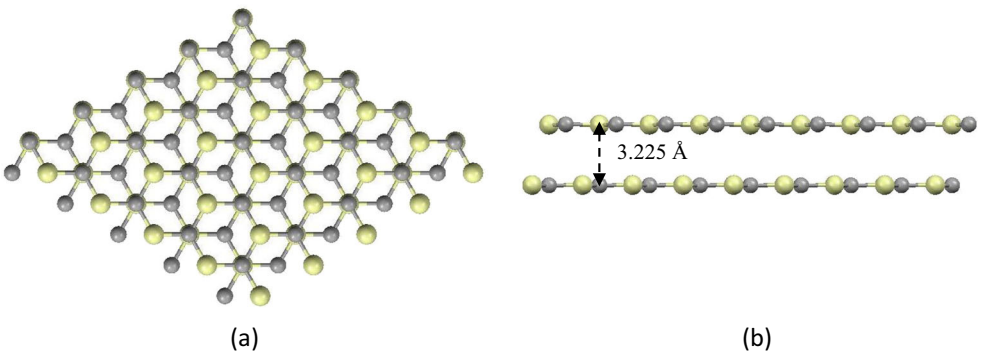


**Fig. 8** Optimized structure and geometrical parameters of Si-C 3layers graphene **a** top view and **b** side view

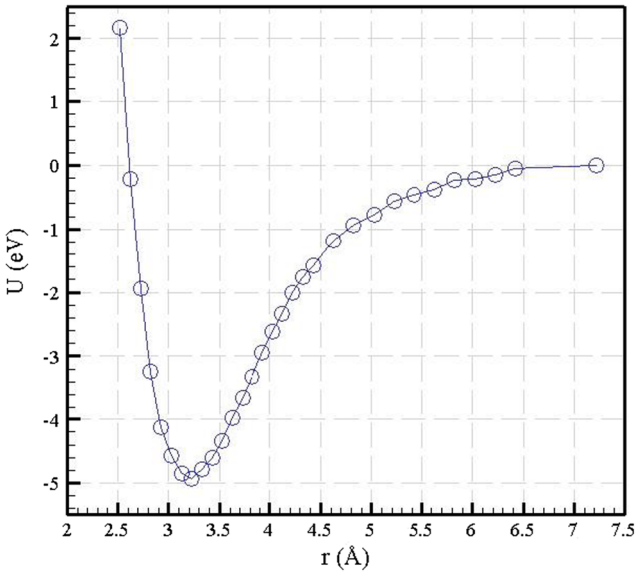


**Fig. 9** potential energy of two monolayer sheets in structure of Si-C bilayers as a function of separation distance

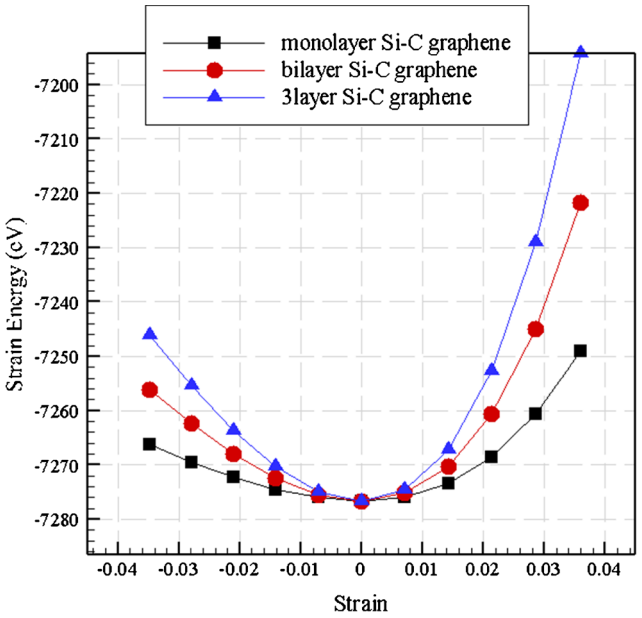


**Fig. 11** Strain energy versus strain for uniaxial strain in monolayer, bilayers and 3layers carbonic graphene sheets

systems over the equilibrium volume, where $\varepsilon$ is the strain [47] as shown in the following equation:

$$E = \frac{1}{V}\left(\frac{d^2E}{d\varepsilon^2}\right)_{\varepsilon=0} \tag{7}$$

We calculated the Young's modulus of carbonic graphene according to Eq. 7, and our results indicate that the Young's modulus values for mono-, bi- and trilayer carbonic graphene sheets were 1.019, 1.016 and 1.015 TPa, respectively. It can be seen from the examination of previous studies that our DFT results are close to the results of other simulation methods such as the continuum model (1.04 TPa) [48], Truss-type analytical models (1.04 TPa) [49], Brenner potential (0.694 TPa) [50], ab initio approach (1.11 TPa) [51], and combination of molecular and solid mechanics (1.06 TPa) [52] and are also in good agreement with experimental results (1.0 ± 0.1 TPa) [53].

## 3.2 Silicon-Carbide Graphene

In this section, we investigated the mechanical and interlayer properties of SiC-graphene. In the structure of SiC-graphene, each carbon atom is connected to a silicon atom by a covalent bond. Figure 7 shows the fully optimized structure of SiC-graphene. It is found that the optimized bond length between carbon and silicon atoms was approximately 1.808 Å, which is in good agreement with the results of a previous study [28]. Moreover, the dimensions of SiC-graphene used in present study were 14.119 Å × 12.168 Å.

Then, another Si-C monolayer sheet was placed on the surface of optimized Si-C graphene based on the two stacking patterns mentioned above. Our DFT calculations indicate that the AB stacking pattern is the favorable geometry for Si-C bilayers, as shown in Fig. 8. This figure shows that the second layer is located at a distance to the

**Fig. 10** Optimized structure and geometrical parameters of Si-C 3layers sheets **a** top view and **b** side view

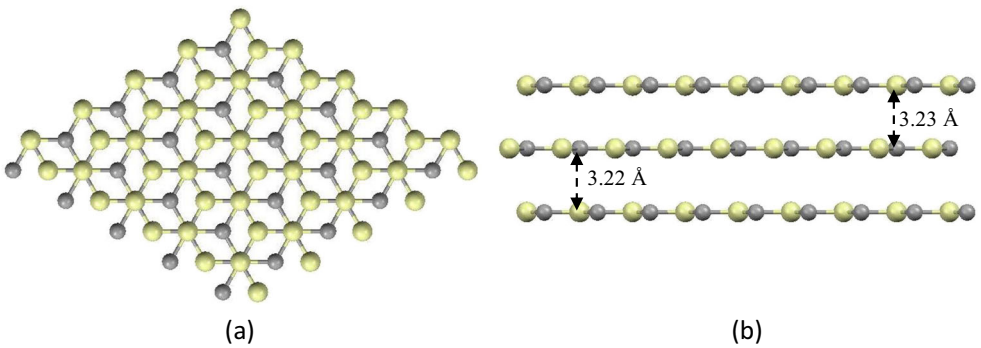

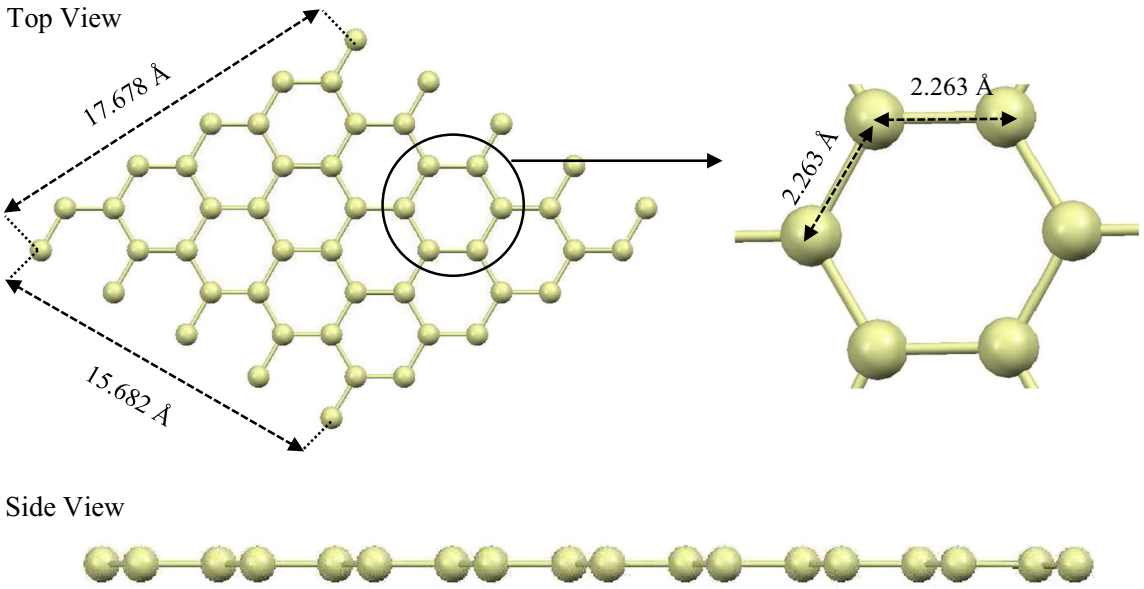


**Fig. 12** Optimized structure and geometrical parameters of Silicene monolayer sheets **a** top view and **b** side view

surface of the Si-C monolayer of 3.225 Å, which is the equilibrium distance in the optimized structure of Si-C bilayers. The adsorption energy between the two layers of this structure was approximately −0.043 eV/bond, corresponding to a strong chemisorption-type adsorption. Moreover, the calculated adsorption energy in the AA stacking arrangement was approximately −0.0144 eV/bond.

To investigate the interfacial interaction between the two layers of Si-C bilayers, we changed the distance between the layers in order to estimate Lennard-Jones parameters according to Eqs. 2–6, and the potential energy between the layers in the Si-C bilayers was plotted as a function of the separation distance, as shown in Fig. 9. The values of the Lennard-jones parameters $\sigma$ and $\varepsilon$ were 2.61 Å and −4.9 eV, respectively.

Next, we placed the monolayer Si-C sheet onto the surface of the Si-C bilayers to investigate the mechanical and electronic properties of the Si-C trilayers. For this purpose, we placed the monolayer sheet on the surface of the Si-C bilayers according to the AB stacking pattern. Figure 10 depicts the optimized structure of the Si-C trilayers, and the corresponding adsorption energy was obtained as −0.055 eV/bond. From this figure it can also be found that the third layers are located on the surfaces of the Si-C bilayers at the equilibrium distance of 3.23 Å.

To evaluate the Young's modulus of the monolayer, bilayers and trilayers of Si-C graphenes, we compressed and then elongated all of these systems in the $x$ direction, as mentioned above, and the strain energy at each strain value was plotted as shown in Fig. 11. Using Eq. 7, the Young's modulus values for the monolayer, bilayer and trilayer of Si-C graphenes were determined to be 0.548, 0.543 and 0.543 TPa, respectively. These results show that the increase in the number of layers did not significantly change the Young's modulus in multilayer SiC graphenes.

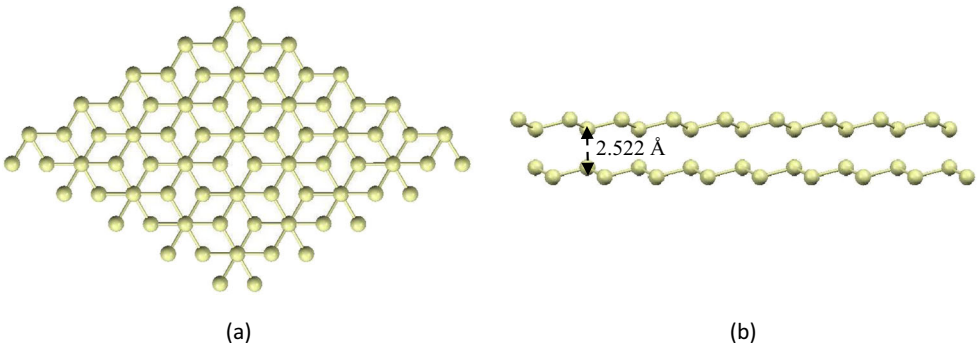


**Fig. 13** Optimized structure and geometrical parameters of Silicene bilayers **a** top view and **b** side view

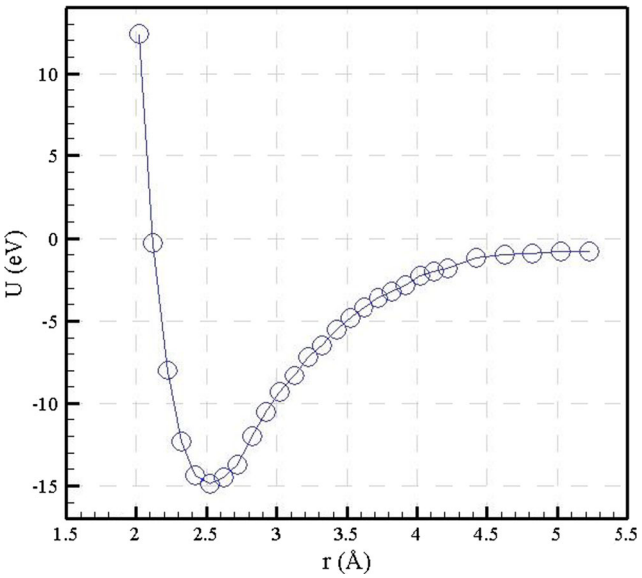


**Fig. 14** Potential energy of two monolayer sheets in structure of Silicene bilayers as a function of separation distance

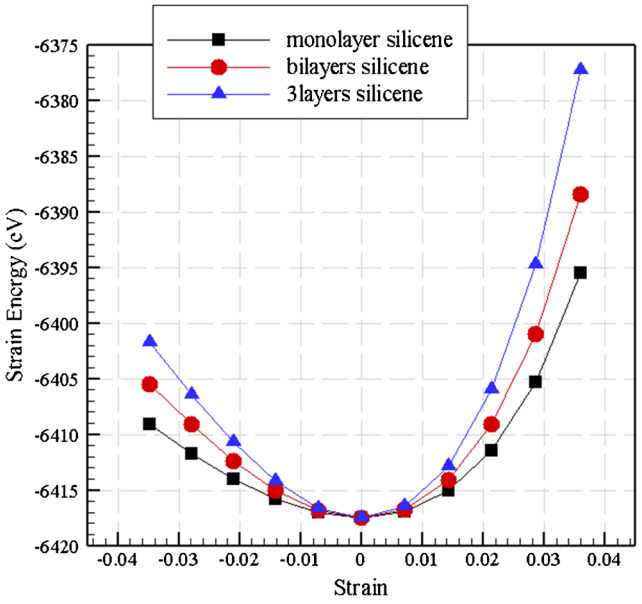


**Fig. 16** Strain energy versus strain for uniaxial strain in monolayer, bilayers and 3layers silicene sheets

### 3.3 Silicene Graphene

In this section, mechanical and interlayer properties of silicene graphene are investigated. First, we optimized the structural geometry of the silicene monolayer sheet as shown in Fig. 12. It can be seen that the equilibrium distance between the two silicon atoms in the silicene monolayer sheet was approximately 2.263 Å. Consideration of previously reported results indicates that our DFT results are in good agreement with a previous modeling study [27]. Furthermore, the dimensions of the silicene monolayer used in the present work were 17.678 Å × 15.682 Å.

Then, another Silicene monolayer sheet was placed on the surface of the first silicene sheet according to the AA and AB stacking patterns. Our DFT results reveal that the first pattern was energetically unstable, and the most stable orientation occurred in the AB arrangement as illustrated in Fig. 13. From this figure, it can be clearly seen that the closest distance between the two silicene monolayers in the silicene bilayer structure was approximately 2.552 Å. Moreover, the adsorbed energy for silicene bilayers in the optimized structure was approximately -0.0128 eV/bond, corresponding to strong chemisorption-type adsorption.

Next, we changed the interlayer distance between the two silicene monolayers in the silicene bilayer structure to evaluate the Lennard-Jones parameters according to Eq. 2–6 as mentioned above. We modeled the interfacial interaction between the two layers using this procedure, and the potential energy between mentioned monolayers was plotted as a function of the separation distance (Fig. 14). The Lennard-Jones parameters $\varepsilon$ and $\sigma$ were equal to −14.89 eV and 2.12 Å, respectively.

Next, a single silicene sheet was placed on the surface of the silicene bilayer according to the AB stacking pattern. The optimized structure of the silicene trilayer is shown in Fig. 15. It can be seen that the interaction energy of the third layer was -0.2626 eV/bond, corresponding to

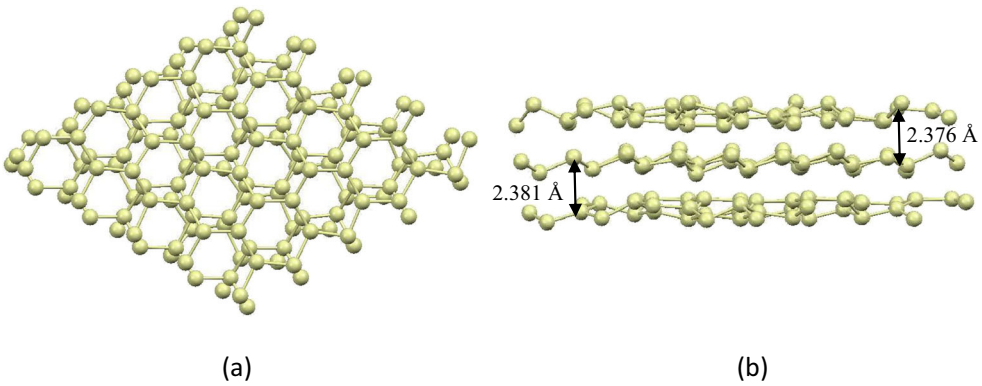


**Fig. 15** Optimized structure and geometrical parameters of Silicene 3layers **a** top view and **b** side view

strongchemisorption-type adsorption. It was also found that the third layer was located on the surface of the bilayers graphene at an equilibrium distance of 2.376 Å.

To calculate the Young's modulus values of mono-, bi- and trilayers of silicene, we compressed and then elongated all of the above-mentioned structures in small increments. The Young's modulus values for mono-, bi- and trilayer silicene obtained using Eq. 7 were approximately 0.296 TPa, 0.193 TPa and 0.181 TPa, respectively. Figure 16 indicates the strain energy at each strain value for the mentioned silicene graphenes. The observed Young's modulus values for carbonic, SiC and silicene graphenes are presented in Table 1. Based on the examination of the data presented in the table, it is concluded that an increase in the number of layers did not clearly change the Young's modulus for C-graphene and SiC, while with the increase in the number of layers to two and three, the mechanical properties for silicene sheets decreased by approximately 35% and 38%, respectively. Thus, these results indicate that the mechanical properties of silicone are more sensitive to the number of layers compared to carbonic or SiC graphenes.

In addition, we investigated the density of states (DOS) as illustrated in Fig. 17 in order to obtain a better understanding of the electronic properties of these systems. According to our calculated DOS plots, carbonic, silicon-carbide and silicene graphene sheets are semiconductors with the HOMO (highest occupied molecular orbital)–LUMO (lowest unoccupied molecular orbital) energy band gaps (Eg) of 3.5, 3.16 and 1.8, respectively. The DOS of multilayer graphenes indicate that with the increase in the number of graphene layers, the band gap energy did not change obviously. For the silicene graphene-like structure, the band gap energy of the monolayer sheet was approximately 1.8 eV. With the increase in the number of layers to two and three layers, the band gap energy first decreased dramatically and reached 0.94 eV, then did not change significantly and reached 0.93 eV. The SiC graphene shows the same electronic behavior. According to above results, the interaction between the silicene layers was stronger than for the other discussed graphenes. The

**Table 1** The Young's modulus of monolayer, bilayers and 3layers of graphenes (TPa)

| Type of graphene | Number of Layer | | |
|---|---|---|---|
| | Monolayer | bilayer | 3layer |
| C- graphene | 1.019 | 1.016 | 1.015 |
| SiC graphene | 0.548 | 0.543 | 0.543 |
| Silicene graphene | 0.296 | 0.193 | 0.181 |

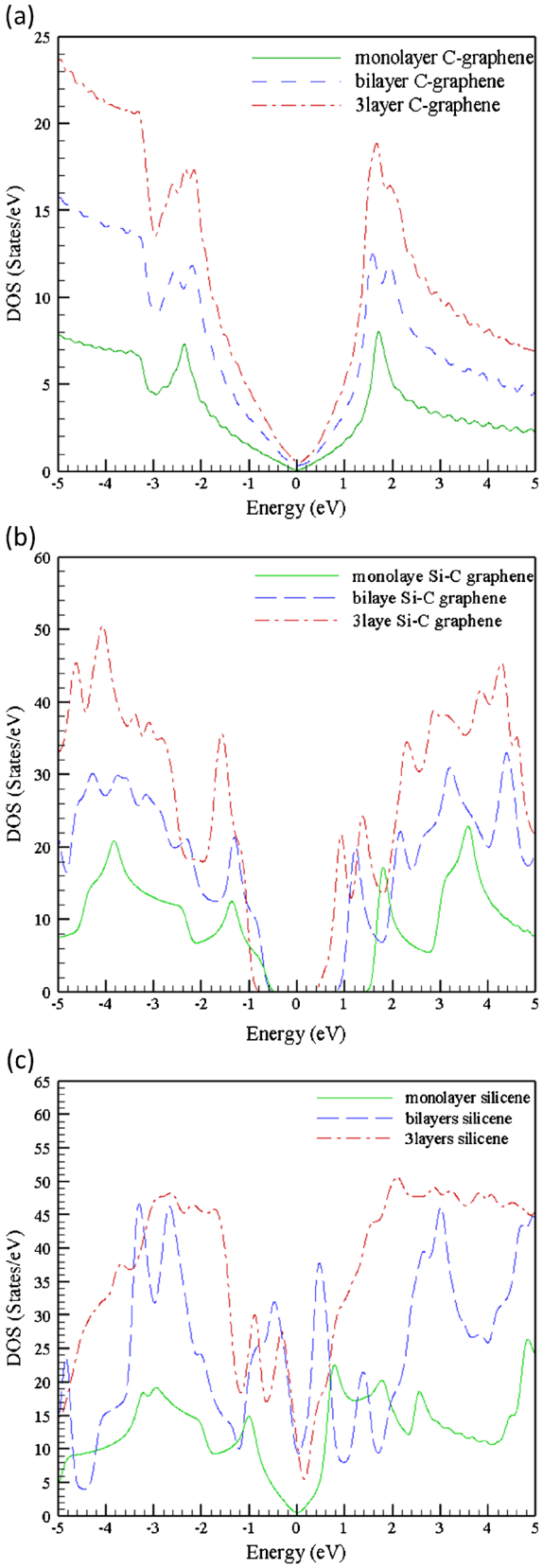


**Fig. 17** Calculated density of sates (DOS) for monolayer, bilayers and 3layers of **a** carbonic, **b** silicon-carbide and **c** Silicene graphene at equilibrium geometry

**Table 2** The energy Band Gap of monolayer, bilayers and 3layers of graphenes (eV)

| Type of graphene | Number of Layer | | |
|---|---|---|---|
| | Monolayer | bilayer | 3layer |
| C-graphene | 3.60 | 3.70 | 3.70 |
| SiC graphene | 3.16 | 2.54 | 2.51 |
| Silicene graphene | 1.80 | 0.94 | 0.93 |

calculated energy band gaps for carbonic, SiC and silicene graphenes sheets are given in Table 2.

The van der Waals interfacial interaction between the two molecules can be represented by a classical linear spring. For example, Ghorbanzadeh [27] replaced the van der Waals interfacial interaction between the polypropylene monomers and silicene graphene sheet with a linear spring with a spring constant of 15.2 $Nm^{-1}$. Examination of the results of previous studies found that the spring constant values, which represented the interfacial interaction between the layers of the boron-nitride, aluminum-nitride and gallium-nitride graphene-like structure, were approximately 87.5938, 1483.379 and 1825.945 $Nm^{-1}$, respectively [46]. The potential equation (2) was Taylor-expanded around the equilibrium distance between the layers of the graphene sheets (measured equilibrium distances of 3.2 Å, 3.225 Å and 2.522 Å for carbonic, SiC and silicene graphenes, respectively) to calculate the spring constant. For small displacements, the terms beyond the third term can be eliminated in a power series. We take the second derivative of the potential energy (2) and obtain:

$$\mathbf{K} = \left(\frac{\mathbf{d^2U}}{\mathbf{dr^2}}|_{\mathbf{req}}\right) = \frac{36\varepsilon}{\mathbf{2^{2/3}}\sigma^{\mathbf{2}}} \tag{8}$$

The spring constants $K$, which can represent the van der Waals interaction between the layers of the carbonic, silicon-carbide and silicene graphene-like structures, are calculated as 92.19, 261.45 and 1230.8 N/m, respectively. From these results, it is concluded that greater adsorbed energy between layers of sheets in multilayer structures results in a stronger modeled spring.

## 4 Conclusions

In summary, in the current work, we employed DFT calculations to investigate the effect of the increase in the number of layers of sheets on the mechanical properties of carbonic, silicon-carbide and silicene multilayer graphene-like structures. Our DFT calculations indicate that the Young's modulus of carbonic and SiC graphenes is independent of the number of layers in multilayer structures, while it is sensitive to the number of layers for silicene. We also found that carbonic graphene had the highest Young's modulus because it had the lowest equilibrium distance between its constituent sheets. Moreover, we modeled the interfacial interaction between the layers in the structures of the studied multilayer graphenes using the Lennard-Jones potential. In addition, we used the Lennard-Jones parameters to model the van der Waals interaction between the layers of multilayer graphenes with a classical linear spring and found that silicene graphene had the highest adsorbed energy between its layers compared to the other studied systems due to its higher spring constant, which was calculated as 1230.8 N/m. Finally, we used the density of states (DOS) plots to gain a better understanding of the electronic properties of the studied graphene layers. These results showed that the increase in the number of layers did not clearly change the band gap energy of C-graphene, while the band gap energy of Si-C graphene and silicene graphene decreased at first and then remained constant and showed that the interaction between the silicene layers was stronger than that of the other studied systems.

## References


1. Iijima S (1991) Helical microtubules of graphitic carbon. Nature 354(6348):56–58
2. Novoselov KS, Geim AK, Morozov SV, Jiang D, Zhang Y, Dubonos SV, Grigorieva IV, Firsov AA (2004) Electric field effect in atomically thin carbon films. Science 306(5696):666–669
3. Mashhadzadeh AH, Vahedi AM, Ardjmand M, Ahangari MG (2016) Investigation of heavy metal atoms adsorption onto graphene and graphdiyne surface: a density functional theory study. Superlattice Microst 100:1094–1102
4. Kroto HW, Heath JR, O'brien SC, Curl RF, Smalley RE (1985) C60: Buckminsterfullerene. Nature 318(6042):162–163
5. Kotov NA (2006) Materials science: Carbon sheet solutions. Nature 442(7100):254–255
6. Lalwani G, Henslee AM, Farshid B, Lin L, Kasper FK, Qin Y-X, Mikos AG, Sitharaman B (2013) Two-Dimensional Nanostructure-Reinforced Biodegradable polymeric nanocomposites for bone tissue engineering. Biomacromolecules 14(3):900–909
7. Shen B, Zhai W, Tao M, Lu D, Zheng W (2013) Chemical functionalization of graphene oxide toward the tailoring of the interface in polymer composites. Compos Sci Technol 77:87–94
8. Stankovich S, Dikin DA, Dommett GHB, Kohlhaas KM, Zimney EJ, Stach EA, Piner RD, Nguyen ST, Ruoff RS (2006) Graphene-based composite materials. Nature 442(7100):282–286
9. Ansari S, Giannelis EP (2009) Functionalized graphene sheet—Poly(vinylidene fluoride) conductive nanocomposites. J Polym Sci B Polym Phys 47(9):888–897
10. Ramanathant AAA, Stankovichs DAD, Herrera Alonso M, Piner RD, Adamson DH, Schniepp HC, Chenx RSR, Nguyen ST, Aksay IA, Prud'homme RK, Brinson LC (2008) Functionalized graphene sheets for polymer nanocomposites. Nat Nano 3(6):327–331

11. Lee YR, Raghu AV, Jeong HM, Kim BK (2009) Properties of waterborne polyurethane/functionalized graphene sheet nanocomposites prepared by an in situ method. Macromol Chem Phys 210(15):1247–1254
12. Xu Y, Wang Y, Liang J, Huang Y, Ma Y, Wan X, Chen Y (2009) A hybrid material of graphene and poly (3,4-ethyldioxythiophene) with high conductivity, flexibility, and transparency. Nano Res 2(4):343–348
13. Quan H, Zhang B-Q, Zhao Q, Yuen RKK, Li RKY (2009) Facile preparation and thermal degradation studies of graphite nanoplatelets (GNPs) filled thermoplastic polyurethane (TPU) nanocomposites. Compos A: Appl Sci Manuf 40(9):1506–1513
14. Eda G, Chhowalla M (2009) Graphene-based composite thin films for electronics. Nano Lett 9(2):814–818
15. Liang J, Xu Y, Huang Y, Zhang L, Wang Y, Ma Y, Li F, Guo T, Chen Y (2009) Infrared-triggered actuators from graphene-based nanocomposites. J Phys Chem C 113(22):9921–9927
16. Fowler JD, Allen MJ, Tung VC, Yang Y, Kaner RB, Weiller BH (2009) Practical chemical sensors from chemically derived graphene. Acs Nano 3(2):301–306
17. Wang Y, Shi Z, Huang Y, Ma Y, Wang C, Chen M, Chen Y (2009) Supercapacitor devices based on graphene materials. J Phys Chem C 113(30):13103–13107
18. Wang C, Li D, Too CO, Wallace GG (2009) Electrochemical properties of graphene paper electrodes used in lithium batteries. Chem Mater 21(13):2604–2606
19. Zhao G, Li X, Huang M, Zhen Z, Zhong Y, Chen Q, Zhao X, He Y, Hu R, Yang T, Zhang R, Li C, Kong J, Xu J-B, Ruoff RS, Zhu H (2017) The physics and chemistry of graphene-on-surfaces. Chem Soc Rev 46(15):4417–4449
20. Hamed Mashhadzadeh A, Fereidoon A, Ghorbanzadeh Ahangari M (2017) Combining density functional theory-finite element multi-scale method to predict mechanical properties of polypropylene/graphene nanocomposites: Experimental study. Mater Chem Phys 201(Supplement C):214–223
21. Yuanbo Z, Angel R, Guy Le L (2017) Emergent elemental two-dimensional materials beyond graphene. J Phys D Appl Phys 50(5):053004
22. Mannix AJ, Kiraly B, Hersam MC, Guisinger NP (2017) Synthesis and chemistry of elemental 2D materials. Nature Reviews Chemistry 1:0014
23. Molle A, Goldberger J, Houssa M, Xu Y, Zhang S-C, Akinwande D (2017) Buckled two-dimensional Xene sheets. Nat Mater 16:163
24. Takeda K, Shiraishi K (1994) Theoretical possibility of stage corrugation in Si and Ge analogs of graphite. Phys Rev B 50(20):14916–14922
25. Leandri C, Lay GL, Aufray B, Girardeaux C, Avila J, Dávila ME, Asensio MC, Ottaviani C, Cricenti A (2005) Self-aligned silicon quantum wires on Ag(1 1 0). Surf Sci 574(1):L9–L15
26. Lalmi B, Oughaddou H, Enriquez H, Kara A, Vizzini S, Ealet B, Aufray B (2010) Epitaxial growth of a silicene sheet. Appl Phys Lett 97(22):223109
27. Ghorbanzadeh Ahangari M (2015) Modeling of the interaction between polypropylene and monolayer sheets: a quantum mechanical study. RSC Advances 5(98):80779–80785
28. Bekaroglu E, Topsakal M, Cahangirov S, Ciraci S (2010) First-principles study of defects and adatoms in silicon carbide honeycomb structures. Phys Rev B 81(7):075433
29. Memarian F, Fereidoon A, Khodaei S, Mashhadzadeh AH, Ganji MD (2017) Molecular dynamic study of mechanical properties of single/double wall SiCNTs: consideration temperature, diameter and interlayer distance. Vacuum 139:93–100
30. Turgut C, Pandiyan S, Mether L, Belmahi M, Nordlund K, Philipp P (2015) Influence of alkane chain length on adsorption on an $\alpha$-alumina surface by MD simulations. Nuclear Instruments and Methods in Physics Research Section B: Beam Interactions with Materials and Atoms 352:206–209
31. Ganji MD, Fereidoon A, Jahanshahi M, Ghorbanzadeh Ahangari M (2012) Elastic properties of SWCNTs with curved morphology: density functional tight binding based treatment. Solid State Commun 152(16):1526–1530
32. Ghorbanzadeh Ahangari M, Fereidoon A, Jahanshahi M, Ganji MD (2013) Electronic and mechanical properties of single-walled carbon nanotubes interacting with epoxy: a DFT study. Physica E: Low-dimensional Systems and Nanostructures 48:148–156
33. Fereidoon A, Ghorbanzadeh Ahangari M, Ganji MD, Jahanshahi M (2012) Density functional theory investigation of the mechanical properties of single-walled carbon nanotubes. Comput Mater Sci 53(1):377–381
34. Sharifi N, Ardjmand M, Ahangari MG, Ganji MD (2013) Si-decorated graphene: a superior media for lithium-ions storage. Struct Chem 24(5):1473–1483
35. Fereidoon A, Mostafaei M, Ganji MD, Memarian F (2015) Atomistic simulations on the influence of diameter, number of walls, interlayer distance and temperature on the mechanical properties of BNNTs. Superlattice Microst 86:126–133
36. Hohenberg P, Kohn W (1964) Inhomogeneous electron gas. Phys Rev 136(3B):B864–B871
37. Kohn W (1999) Nobel lecture: electronic structure of matter\char22()wave functions and density functionals. Rev Mod Phys 71(5):1253–1266
38. Ordejón P, Artacho E, Soler JM (1996) Self-consistent order-$,N$ density-functional calculations for very large systems. Phys Rev B 53(16):R10441–R10444
39. José MS, Emilio A, Julian DG, Alberto G, Javier J, Pablo O, Daniel S-P (2002) The SIESTA method for ab initio order- N materials simulation. J Phys Condens Matter 14(11):2745
40. Jafari SA, Jahanshahi M, Ahangari MG (2017) Platinum adsorption onto graphene and oxidized graphene: a quantum mechanics study. Mater Chem Phys 190:17–24
41. Ganji MD, Sharifi N, Ahangari MG (2014) Adsorption of H2S molecules on non-carbonic and decorated carbonic graphenes: a van der Waals density functional study. Comput Mater Sci 92:127–134
42. Ghorbanzadeh Ahangari M, Fereidoon A, Hamed Mashhadzadeh A (2017) Interlayer interaction and mechanical properties in multilayer graphene, Boron-Nitride, Aluminum-Nitride and Gallium-Nitride graphene-like structure: a quantum-mechanical DFT study. Superlattice Microst 112(Supplement C):30–45
43. Kan E, Ren H, Wu F, Li Z, Lu R, Xiao C, Deng K, Yang J (2012) Why the band gap of graphene is tunable on hexagonal boron nitride. J Phys Chem C 116(4):3142–3146
44. Wang Y, Ding Y (2013) Structural, electronic, and magnetic properties of the semifluorinated boron nitride bilayer: a first-principles study. J Phys Chem C 117(6):3114–3121
45. Memarian F, Fereidoon A, Darvish Ganji M (2015) Graphene Young's modulus: Molecular mechanics and DFT treatments. Superlattice Microst 85:348–356
46. Ghorbanzadeh Ahangari M, Fereidoon A, Hamed Mashhadzadeh A (2017) Interlayer interaction and mechanical properties in multilayer graphene, Boron-Nitride, Aluminum-Nitride and Gallium-Nitride graphene-like structure: a quantum-mechanical DFT study Superlattices and Microstructures
47. Zhou G, Duan W, Gu B (2001) First-principles study on morphology and mechanical properties of single-walled carbon nanotube. Chem Phys Lett 333(5):344–349

48. Shokrieh MM, Rafiee R (2010) Prediction of Young's modulus of graphene sheets and carbon nanotubes using nanoscale continuum mechanics approach. Materials & Design 31(2):790–795
49. Scarpa F, Adhikari S, Phani AS (2009) Effective elastic mechanical properties of single layer graphene sheets. Nanotechnology 20(6):065709
50. Huang Y, Wu J, Hwang KC (2006) Thickness of graphene and single-wall carbon nanotubes. Phys Rev B 74(24):245413
51. Van Lier G, Van Alsenoy C, Van Doren V, Geerlings P (2000) Ab initio study of the elastic properties of single-walled carbon nanotubes and graphene. Chem Phys Lett 326(1–2):181–185
52. Natsuki T, Tantrakarn K, Endo M (2004) Prediction of elastic properties for single-walled carbon nanotubes. Carbon 42(1):39–45
53. Lee C, Wei X, Kysar JW, Hone J (2008) Measurement of the elastic properties and intrinsic strength of monolayer graphene. Science 321(5887):385–388